Structure
Article

Cryo-EM Structure of a Molluscan Hemocyanin Suggests Its Allosteric Mechanism

Qinfen Zhang,[1,2] Xinghong Dai,[1] Yao Cong,[2,3] Junjie Zhang,[2,5] Dong-Hua Chen,[2] Matthew T. Dougherty,[2] Jiangyong Wang,[4] Steven J. Ludtke,[2] Michael F. Schmid,[2] and Wah Chiu[2,*]
[1]State Key Laboratory of Biocontrol, School of Life Sciences, Sun Yat-sen University, Guangzhou 510275, China
[2]National Center for Macromolecular Imaging, Verna and Marrs McLean Department of Biochemistry and Molecular Biology, Baylor College of Medicine, Houston, TX 77030, USA
[3]State Key Laboratory of Molecular Biology, Institute of Biochemistry and Cell Biology, Shanghai Institutes for Biological Sciences, Chinese Academy of Sciences, Shanghai 200031, China
[4]South China Sea Fisheries Research Institute, Chinese Fisheries Academy, Guangzhou 510300, China
[5]Present Address: Department of Structural Biology, Stanford University, Stanford, CA 94305, USA
*Correspondence: wah@bcm.edu
http://dx.doi.org/10.1016/j.str.2013.02.018

SUMMARY

Hemocyanins are responsible for transporting O_2 in the arthropod and molluscan hemolymph. *Haliotis diversicolor* molluscan hemocyanin isoform 1 (HdH1) is an 8 MDa oligomer. Each subunit is made up of eight functional units (FUs). Each FU contains two Cu ions, which can reversibly bind an oxygen molecule. Here, we report a 4.5 Å cryo-EM structure of HdH1. The structure clearly shows ten asymmetric units arranged with D5 symmetry. Each asymmetric unit contains two structurally distinct but chemically identical subunits. The map is sufficiently resolved to trace the entire subunit Cα backbone and to visualize densities corresponding to some large side chains, Cu ion pairs, and interaction networks of adjacent subunits. A FU topology path intertwining between the two subunits of the asymmetric unit is unambiguously determined. Our observations suggest a structural mechanism for the stability of the entire hemocyanin didecamer and 20 "communication clusters" across asymmetric units responsible for its allosteric property upon oxygen binding.

INTRODUCTION

Molluscan hemocyanins (MHs) are large macromolecular assemblies relevant to molecular evolution and have biotechnological and therapeutic applications (Altenhein et al., 2002; Burmester, 2001; Kröger et al., 2011; Lieb et al., 2001; van Holde et al., 2001). The Keyhole limpet hemocyanin (KLH), one type of MH, is large in size and has numerous epitopes, which efficiently elicit the immune response for vaccines of several blood, skin, breast, and bladder cancers (Longenecker et al., 1993; Helling et al., 1994). In addition, specific tumor-associated antigens can be conjugated to KLH to stimulate antitumor immune responses (Longenecker et al., 1993; Sabbatini et al., 2007; Slovin et al., 2005). High-resolution structure of the intact Molluscan hemocyanin will provide the more complete structural information to inspire design options of more effective vaccines.

MHs are divided into two subclasses: the exclusively decameric cephalopod hemocyanins and the predominantly didecameric gastropod hemocyanins (Keller et al., 1999). It generally consists of 10 or 20 subunits of ~400 kDa per subunit. Each subunit is folded into seven or eight successively linked functional units (FUs) with ~45% protein sequence identity among them (Lieb et al., 2001) and conventionally named as FU-A to FU-G or FU-A to FU-H.

FU arrangement in MHs has been previously investigated by means of immunoelectron microscopy and cryo-electron microscopy (cryo-EM) (Gatsogiannis and Markl, 2009; Gatsogiannis et al., 2007; Gebauer et al., 1999, 2002; Harris et al., 1993; Lamy et al., 1998), and a model was proposed (Gatsogiannis and Markl, 2009; Meissner et al., 2007). In that model, the dimeric subunits within an asymmetric unit interact with each other mainly through their FU-E and FU-F. However, this model cannot adequately explain the results of several biochemical experiments, which demonstrated that MHs disassemble into dimers instead of individual subunits when either bivalent metal ion (such as Ca^{2+}, Mg^{2+}, etc.) concentration is reduced or pH is increased (Harris et al., 2004; Siezen and van Bruggen, 1974; Siezen and van Driel, 1974).

As a distinct class of oxygen-transport metalloproteins, physiological measurements have demonstrated lower cooperativity of oxygen binding in MHs (van Holde et al., 2000). A hypothesis based on comparison of crystal structures of single MH FU with and without oxygen has been proposed to explain how the conformational changes induced by oxygen binding or release are communicated between FUs to produce positive cooperativity (Perbandt et al., 2003). However, how the FUs in the entire MH assembly communicate and respond upon ligand binding and why the oxygen-binding cooperativity in MHs is low remains unclear.

Here, we report a 4.5 Å resolution cryo-EM map of *Haliotis diversicolor* hemocyanin isoform1 (HdH1) and a corresponding Cα model derived from flexible fitting of a comparative model with the constraints of the density map. Our study concludes a different path of FU arrangement in the native oligomer as compared to the previous models (Gatsogiannis and Markl, 2009; Gatsogiannis et al., 2007; Meissner et al., 2007).

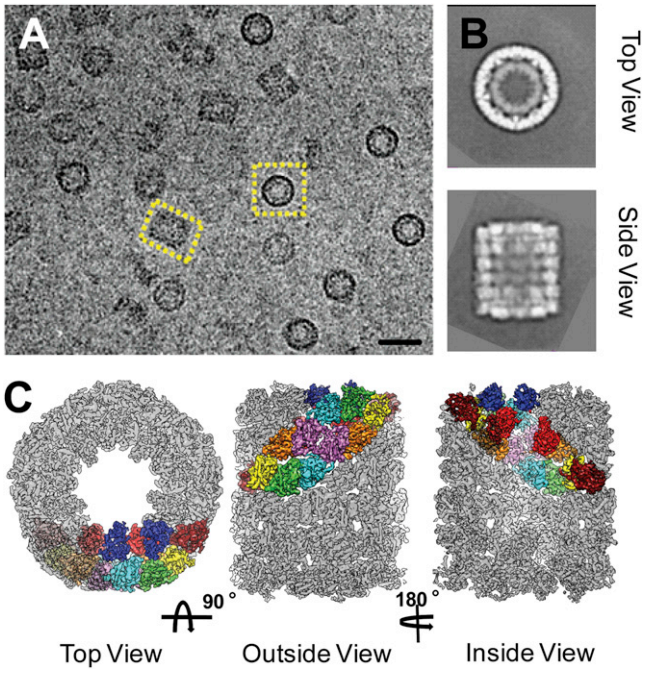

Figure 1. Structure of the HdH1

(A) Representative cryo-EM micrograph of the HdH1. The yellow frames highlight top and side views of the complex (scale bar, 500 Å).

(B) Reference-free 2D averaged images of the representative top and side views.

(C) Top view, exterior side view, and cutaway interior view of the HdH1 density map. One asymmetric unit is highlighted in color. Each of the eight FUs in one subunit of the asymmetric unit is colored differently (FU-A, dark red; FU-B, yellow; FU-C, lime green; FU-D, orange; FU-E, orchid; FU-F, cyan; FU-G, red; FU-H, blue). Since there are two chemically identical subunits within one asymmetric unit, the corresponding FUs in both subunits are colored the same. The top view reveals that, in one subunit, in addition to the six FUs located in the outer wall of the cylinder (see the exterior side view), the remaining two FUs (FU-G in red and FU-H in blue) can be seen in the cutaway inside view and are attached to the interior of the outer wall (Movie S1). The color schemes for each FUs are the same throughout this paper.

See also Figure S1.

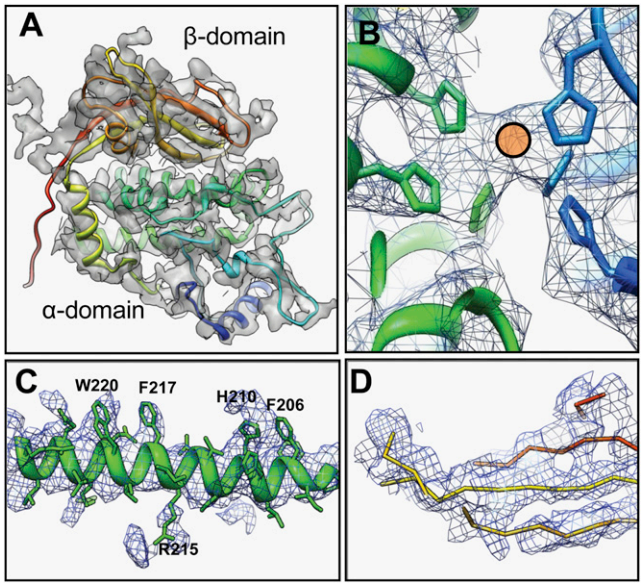

Figure 2. High-Resolution Structural Features of the HdH1 Cryo-EM Density Map

(A) Taking FU-A1 as an example, the overall comparative model fits well into the corresponding map as a rigid body, which validates the quality of our map; however, the C-terminal linker and some of the loop regions of the comparative model are not well fitted into the map and require further refinement. The model is shown in rainbow color with the N-terminal in blue and the C-terminal in red.

(B) Zoom-in view of the organization of the active center in the α-domain of FU-A1. The active center of every FU in our map can be easily found. Without any adjustment, the side chains of the six His (stick models) surrounding the active center can be easily fit into the densities. The orange disk marks the extra density between the His, which likely belongs to the density of the di-copper ions.

(C) A representative α helix in our map. Blue wire shows the density and the green ribbon shows the comparative model by rigid-body fitting. Some bulky side chains, for example, the His, Arg, Trp, and the Phe, can be observed.

(D) The β strand separation is discernible in this map.

See also Figure S2.

RESULTS

3D Reconstruction and the Overall Structure of HdH1

Sixty-five thousand HdH1 particle images were picked from 832 electron micrographs (Figure 1A) with defocus values ranging from 0.6 to 2.6 μm. About 70% of the micrographs contain usable contrast beyond 4 Å resolution (Figures S1A and S1B available online). EMAN1 was used for all image processing (Ludtke et al., 1999). Reference-free 2D analysis of the particle images exhibits views indicating an overall D5 symmetry (Figures 1B and S1C), which was subsequently imposed in the 3D reconstruction process. Particle images (28,641) were retained in the final reconstruction, and the resolution of the final density map was assessed to be 4.5 Å based on the 0.5 Fourier Shell Correlation (FSC) criterion (Saxton and Baumeister, 1982; Harauz and Van Heel, 1986) (Figure S1D).

Our map shows that HdH1 consists of two opposing cylindrical decamers (Figure 1C). Each decamer consists of five asymmetric units, each asymmetric unit consisting of a dimer of subunits (Figure 1C in color). In each subunit, there are eight FUs (Figure 1C; Movie S1). All the HdH1 FUs bear a relative high protein sequence identity (40%∼57%) to the FU-G of *Octopus dofleini* hemocyanin whose crystal structure is known (Odg, Protein Data Bank [PDB] ID: 1JS8) (Cuff et al., 1998). This allowed us to build a comparative model for each FU using Modeller (Sali and Blundell, 1993) from the sequence of HdH1 and the structure of Odg.

Backbone Topology Trace of the Eight FUs in a Single Subunit

Each functional unit contains two structural domains: the α-domain, rich in α helixes, and the β strand domain. Overall fit of the comparative models appears good for most of the FU densities except for their loop and linkers regions (Figure 2). In some regions, protruding densities are visible and match with the corresponding bulky side chains in the sequence (Figures 2B and 2C; Table S1).

The core of each FU (excluding the linker density) was segmented out by matching the comparative model with our

density map using UCSF *Chimera* (Pettersen et al., 2004). Each FU is composed of an N-terminal α-helical domain and a C-terminal β sandwich domain (Figure 2A). The long linking densities between connecting FUs were then determined based on the locations of the C terminus of one FU and the N terminus of the consecutive FU (Movie S2). The FUs are designated as FU-A1 to H1 for one subunit and A2 to H2 for the other subunit within the asymmetric unit according to the nomenclature of previous literature (Gatsogiannis and Markl, 2009). Different colors are chosen for each FU to facilitate its identity within a subunit (Figure 1C). Six FUs (A–F) form the outer wall of the cylinder, while the remaining two (G and H) are attached to the inside of the outer wall (Figure 1C; Movies S1 and S2).

Map Quality Assessment and Model Optimization

High-Resolution Features

At 4.5 Å resolution, our cryo-EM density map reveals essential structural details not seen in any previous studies of the entire native MH complex (Gatsogiannis and Markl, 2009; Gatsogiannis et al., 2007; Meissner et al., 2007; Lieb et al., 2010). The pitches of α helices (Figure 2C), separation of β strands (Figure 2D), boundary of each FU, most of the connections between consecutive FUs, and several bulky side chains are discernable in our density map (Figure 2).

Reliability of the Density Evidenced in the Two Subunits in an Asymmetric Unit

Because there are two chemically identical subunits per asymmetric unit and we did not impose any symmetry between them during data processing, the segmented densities of the two subunits can be considered as two independent structural determinations of the same protein. Therefore, a comparison of their structures would provide a strong indication of the reliability of the observed features in the corresponding regions of the two subunits. To verify this correspondence quantitatively, we computed the FSC of the 3D densities of all of the corresponding FUs between the two subunits (Figures S1E and S1F). This pairwise comparison confirms the high structural similarities between the corresponding FUs. The best correlation occurs in FUs D1 and D2 pair and FUs E1 and E2 pair, with 0.5 FSC at 5.0 Å and 0.143 FSC at 4.0 Å resolution. The lowest resolution in the FSC measurement, between the H1 and H2 pair, is possibly caused by their loose attachment to the outer wall.

Resolvability of Side-Chain Density

Reliability in recognizing side chains can be judged by the match of side-chain size and shape between the model and the map. There are about 360 amino acids in the core region of each FU (i.e., not counting the linker regions). Among them, more than 40% of the amino acids sequence is identical to the FU-G of *Octopus dofleini* hemocyanin, whose X-ray structure is available (Odg, PDB ID: 1JS8). Taking FU-A1 as an example, there are 167 amino acids identical to that of Odg. Among these conserved amino acids, we examined the visibility of several types of small and bulky side chains in the expected locations in the map using the same density threshold. We selected Ala and Gly, which are small side chains, as negative controls and His, Tyr, Trp, Arg, Phe, Lys, Glu, and Gln, which are bulky side chain, as the candidates likely to be visible. The choice of these conserved amino acids for examination was made because they are likely to be well packed and rigid, therefore, likely adopting the same spatial configuration (Summers et al., 1987).

As expected from the estimated resolution of the map (Figures S1D and S1E), we cannot find any obvious protruding density for Ala and Gly in our map. Conversely, for amino acids with bulky side chains, they are visually apparent in both copies of each FU as exemplified in a helical segment in Figure S2A. This density similarity also extends to the eight pairs of Cu ion binding sites and their local environments, which include six His in each site (Figures 2B and S2B). Furthermore, after a visual count on the visibility of the bulky side chain residues, such as His, Tyr, Trp, Phe, Arg, Lys, Glu, and Gln, in FU-A1 (Table S1), we can conclude that for the negative control small amino acids, 100% of them are true negatives in our map. For the amino acids with bulky side chain, all His and Trp and two-thirds of the Tyr and Phe can be positively identified in our map, while several Arg and Lys side chains cannot be unambiguously identified because they are located in the relative dynamical loop regions. Taken together, this statistical analysis in the resolvability of the bulky side-chain densities matches the expectation from a density map determined at 4.5 Å resolution.

Model Optimization

The initial comparative models for FUs were first rigid-body-fitted into the density map, which can already fit the cores of the FUs well except for some loop regions (Figure 2A). Further loop refinement of those regions was initially carried out with Modeller (Sali and Blundell, 1993) and was subsequently adjusted by Coot (Emsley and Cowtan, 2004) particularly for the loop and linker regions. Finally, Rosetta (DiMaio et al., 2009) was used to perform a global flexible fitting of the model to the density for each FU and a simultaneous optimization of protein geometry. After these steps, we connected all the FUs' models in each subunit and did some minor local adjustments around the linkers using Coot. The resulting models show good match with the experimental densities including the linker regions for the entire subunits (Figure S3; Movie S2).

DISCUSSION

Single-particle cryo-EM has been used to determine structures of a number of large macromolecular machines to near atomic resolution. Several cases, in which X-ray structures have also been solved, confirmed the reliability of the EM maps and associated models (Ludtke et al., 2008; Zhang et al., 2008). The validation of the map of HdH1 is supported by (1) the remarkable match between the model and the protruding densities for some of the putative bulky side chains, and (2) the high structural correlation (FSC) between corresponding FUs in the two independent subunits within the asymmetric unit (Figures S1E, S1F, and S2). It is recently recognized that the commonly used even-odd FSC = 0.5 resolution test of two subsets of particle images split after a common refinement process (Figure S1D) may not be an accurate estimate of true map resolution (Scheres and Chen, 2012). In this study, we performed another resolution test based on the comparison of eight pairs of equivalent FUs in the asymmetric unit (Figures S1E and S1F). Since they are not symmetry related to each other, the corresponding FU densities can be considered as independently determined. The resolutions of the corresponding FUs are estimated to range from

4.0 to 5.3 Å at the 0.143 FSC threshold (Rosenthal and Henderson, 2003). These analyses show the map resolution is not uniform throughout the entire map. The well-packed and rigid FUs are better resolved than the loosely connected ones at the terminus of the subunit.

Furthermore, unambiguous visualization of α helix pitches and β strand separation (Figures 2C and 2D) and the match of the comparative model to the map provide compelling evidences for the map quality. While we cannot resolve all side chains in our map, the comparative modeling of each FU and the unambiguous connectivity between adjacent FUs have allowed us to describe the key residues involved in subunit interactions rather confidently. This structural information can thus yield mechanistic insight into subunit assembly and explain biochemical phenomenon related to subunit cooperativity upon O_2 binding.

Completing the Cα Trace of the Single Subunit

The quality of our map and the well-fitted models allow us to build models of each FU for both subunits in an asymmetric unit. The arrangement of FU-A to FU-F is similar between the two subunits; however, the organizations of FU-F and FU-G are quite different in the two subunits (Figure 3). Furthermore, our map clearly depicts most of the densities connecting two consecutive FUs, except for the linker between FU-G2 and FU-H2. However, this last connection can be deduced because it is the only remaining option. Furthermore, each linker density has the proper length to accommodate the sequence of the corresponding inter-FU loop in our model (Movie S2). These loops are mostly in an extended conformation (Figure 3). These features support our assignment of the FUs and their linkers. Finally, the Cα trace in each of the two subunits in an asymmetric unit can be completed.

Organization of the Subunit Dimer in the Asymmetric Unit of HdH1

With assignment of every FU, the relationship between the two subunits in the asymmetric unit can be determined. After aligning both subunits in the same orientation (Figure 3), it becomes obvious that the relationships of A1 through F1 and A2 through F2, which are located in the outer wall of the cylinder, are related by a pseudo 2-fold symmetry; however, the G and H FUs of the two subunits, which are inside the cylinder, are oriented differently (Figure 3; Movie S1).

Each of the FUs can fold independently as evidenced by the fact that single FUs can be disassociated and isolated from the whole complex and crystallized (Cuff et al., 1998; Perbandt et al., 2003). Each FU has enough length in its linker regions to accommodate the various spatial and orientational differences between successive FUs as shown in Figure 3. Once the dimer is formed, dimers can interact with each other as relatively independent and rigid entities, forming a hierarchy of associations all the way to the didecamer. This makes sense from the points of view of single protein subunit folding and subunit-subunit interactions.

The observed FU connectivity leads to a subunit model (Figure 4) that is different from the previously suggested one (Gatsogiannis and Markl, 2009; Gatsogiannis et al., 2007). In both models the same path from A to D is followed (Figure S4A); however, FU-D is connected to the FU-E with about 45° turn in our model instead of the other copy of FU-E in front of FU-D in the previous model (Figures 4 and S4A). This single difference leads to a completely different subunit interaction patterns in the two models. According to the previous model, the intersubunit interactions in an asymmetric unit resided between FU-E and FU-F (i.e., FU-E1 and FU-F2; FU-E2 and FU-F1) and the pair of FU-Es (i.e., FU-E1 and FU-E2). However, in our model, the two subunits in an asymmetric unit are "intertwined" and form a tightly bound dimer. Importantly, our model reveals additional interactions between FU-E1 and FU-D2; FU-F1 and FU-C2 and their reciprocals (i.e., FU-E2 and FU-D1; FU-F2 and FU-C1). Furthermore, by fitting our model to the previous reported 9 Å KLH density map (Gatsogiannis and Markl, 2009, EMD database accession number: EMD-1569), we found our model can fit their density very well including the linker densities between the FU-D and FU-E which were ignored in their modeling (Figure S4B).

Although our and previous models are both consistent with previous immunoelectron microscopy studies (Harris et al., 1993), the previous model could not satisfactorily explain several biochemical experiments demonstrating that MHs disassembled into dimers instead of single subunits (Harris et al., 2004; Siezen and van Bruggen, 1974; Siezen and van Driel, 1974). Based on our intertwined model of the dimeric subunits in an asymmetric unit, we can rationalize that they would correspond to the observed dimer in the biochemical experiments.

Subunit Interactions between the Two Decamers

Our map also allows us to analyze the interface region between the two decamers, where ten connections with high density are observed (Figure 5A). Each of these regions is formed between a long loop of FU-A1 in one decamer and a short turn of FU-B1 in the opposite decamer.

Metal ions have been shown biochemically to be essential for maintaining the didecameric state of gastropod hemocyanins (Harris et al., 2000). In the crystal structure of *Rapana thomasiana* hemocyanin FU-E (RtH2e), a metal ion was identified to participate in the subunit-subunit interaction. Three residues, including a His and an Arg from one subunit and a His from another symmetry-related subunit, are involved in chelating the metal ion (Perbandt et al., 2003). In HdH1, our model places residues Asp269, Tyr270, and His271 in FU-A1 (or FU-A1′) and Arg722, His725, Glu726, and Arg727 in FU-B1′ (or FU-B1) near these didecamer interfaces. Therefore, these relatively high and bulky densities (indicated by arrowhead in Figure 5A) may contain not only the bulky side chains (e.g., Arg, Tyr, and His) but also the ionic elements such as Ca^{2+} or Mg^{2+} (Harris et al., 1997). They may play a key role in the didecamer assembly and stability.

Previous cryo-EM studies suggested several other interactions at the interface of the two decamers (Gatsogiannis and Markl, 2009). However, besides the above-observed interactions, our map shows only tenuous interactions between FU-C1 and FU-F2′ (or FU-C1′ and FU-F2) of the two decamers (Figure 5B).

Intersubunit Communication upon Oxygen Binding

Vertebrate hemoglobin is usually taken as an archetype of the allosteric effect, wherein the binding of oxygen to one subunit of the tetrameric hemoglobin affects the binding affinity of

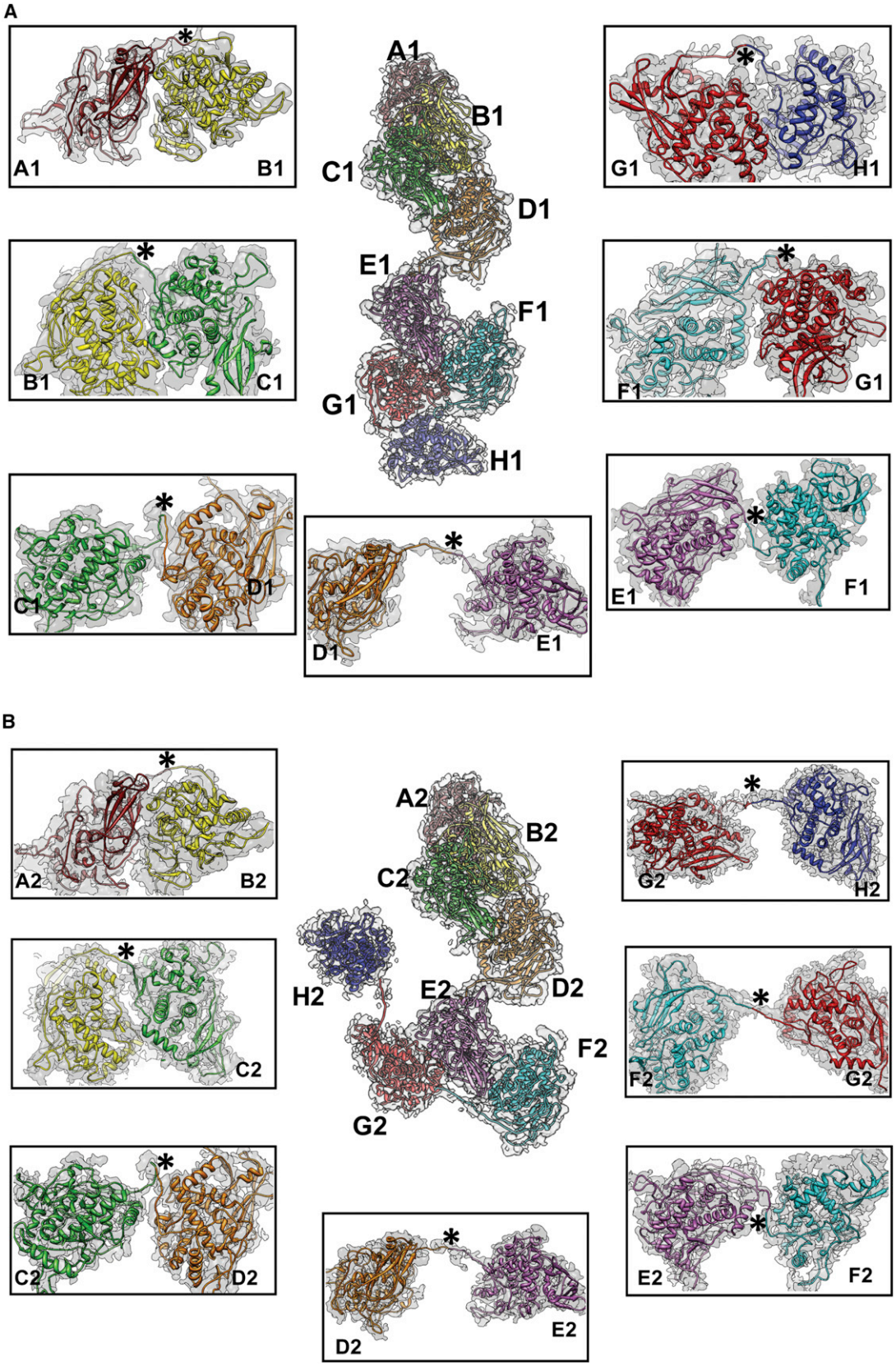

(legend on next page)

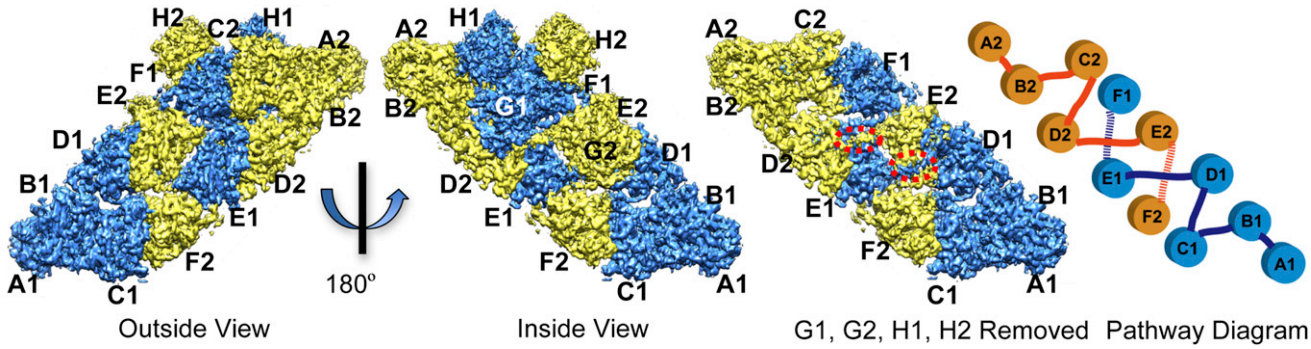

Figure 4. FU Arrangement in an Asymmetric Unit

The two subunits of one asymmetric unit are shown in blue and yellow, respectively.

Outside and inside view of the asymmetric unit with the FUs being labeled. For the inside view, after removing the density of the inner layer (FUs-G1, G2, H1, and H2), the linker between FU-D1 and E1 and that between FU-D2 and E2 can be clearly observed (highlighted by dotted red ovals). The density map clearly depicts an "intertwined" pattern formed by FU-D1E1F1 and FU-D2E2F2, which is illustrated in a cartoon diagram of the FU arrangement pathway on the right. Our linkage pathway is different from that of a previous model (Gatsogiannis and Markl, 2009; Meissner et al., 2007), which would link D1 to E2 and D2 to E1 (Figure S4).

See also Figure S4 and Movie S2.

oxygen to the other subunits. Specific subunit-subunit interactions and communications are responsible for this allosteric behavior. Molluscan hemocyanin has the same function as that of hemoglobin. There are many interfacial contacts between neighboring FUs within and across subunits in MHs (Figures 5, 6, and S5). But most of them do not have a direct linkage to the residues at the ligand binding sites and could not attribute directly to the allosteric behavior.

It is well established that there is only one oxygen-binding site per FU and each oxygen-binding site includes six highly conserved His (for example, His41, His61, His70, His181, His185, and His 212 in one FU of RtH2e). In the crystal structure of a single FU-E (RtH2e) (Perbandt et al., 2003), the loop residues 47–60 in the α helix domain of one FU makes contacts with the β domain of another FU. Cys59 in this loop forms a thioether bond with His61 in the oxygen-binding center. In addition, Leu343 in the β sandwich domain of another FU was found to interact with His185 also in the oxygen-binding site. Therefore, the interface residues are closely coupled to the His residues in the oxygen-binding site of respective FUs. These couplings have been suggested to be involved in the cooperative effects of the oxygen binding and release (Perbandt et al., 2003).

In HdH1, the residues of Cys in the loop and Leu in the β sandwich domain are highly conserved among hemocyanins. However, we do not find the same type of interfacial interactions within the FUs of a single subunit or between subunits in an asymmetric unit involving these residues that are concurrently linked to the residues in the oxygen-binding pocket as based on crystal structure of a single FU. However, we have found a similar type of interfacial interactions between the FUs of subunits of neighboring asymmetric units, for instance, FU-E1 of one subunit and FU-A1* of another subunit in the neighboring asymmetric unit (designated with *), and similarly for the D2-B1*, E2-A2*, and D1-B2* pairs (black arrows in Figure 6). Between two decamers, FU-C1 and FU-F2′ also potentially form similar interaction, but they appear to be more tenuous (Figure 5B). In addition, we found interactions between the two β sandwich domains from FUs of different asymmetric units (red arrows in Figure 6), each of which is connected to the oxygen-binding center via Leu as seen in the RtH2e crystal structure. Therefore, the FU-A1* and FU-B1* of one asymmetric unit and FU-D2, E1 in another asymmetric unit can group together to form a "communication cluster" through these two types of interactions. Symmetrically, FU-A2* and FU-B2* of one asymmetric unit and FU-D1, E2 in the neighboring asymmetric unit can be grouped together to form another "communication cluster" (Figure 6).

Although HdH1 has 20 subunits and 160 FUs, our structure shows various types of FU-FU interactions as shown in Figures 5, 6, and S10. Only the FUs involved in the mentioned "communication cluster" are directly involved in the cooperativity of oxygen binding and release because the interfacial residues are also linked to the residues in the oxygen-binding pocket. The other FUs would not be directly involved in the cooperativity. Because of the D5 symmetry of the complex, there are 80 FUs, which are grouped into 20 independent "communication clusters." Furthermore, there is no apparent communication between the different "communication clusters." Our interpretation of the allosteric effects in terms of "communication cluster"

Figure 3. Linkers between the Neighboring FUs

(A) and (B) show the FU linkers in the two different subunits within one asymmetric unit, respectively. The central panel shows the overall organization of the eight FUs in one asymmetric unit with the map in gray and different FU models in different colors as in Figure 1. FU-A through FU-F in the central panel of (A) and (B) have been rotated to have the same orientation for easy comparison. Surrounding panels around the central panel show consecutive pairs of FUs and the linkers between them indicated by black asterisks. Each panel may have different scales. Most linker densities are clearly observed, for example, the linker between D1 and E1 and between D2 and E2. However, some linker densities have weaker connectivity (for example, G1–H1 and G2–H2).

See also Figure S3 and Movie S2.

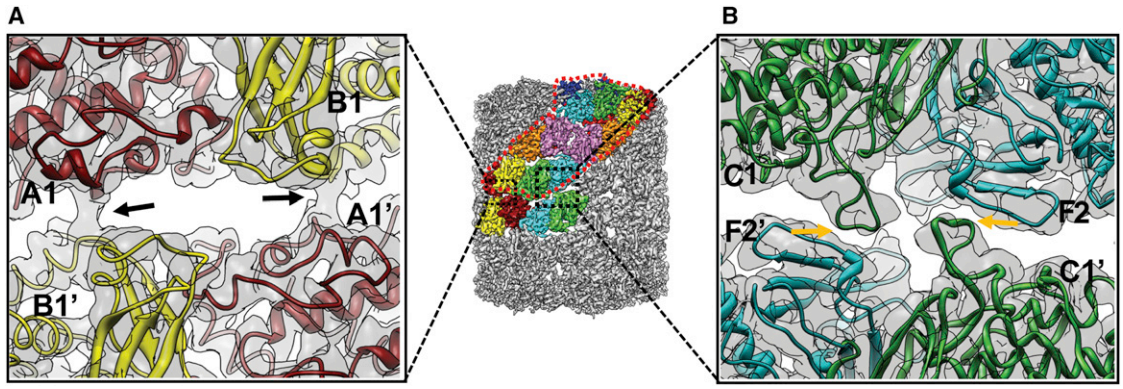

Figure 5. Interactions in the Interface between the Two Decamers in HdH1

(A) There are strong extra densities (highlighted by black arrows) at the interface between the two decamers, showing the intensive interactions between FU-A1 in one decamer and FU-B1 in the other one. A1 and B1 indicate the two FUs belong to one decamer while A1′ and B1′ belong to another decamer. There are ten such strong interaction sites in this interface.

(B) In addition, there are weaker interactions between FU-C of one decamer and FU-F of the other in the decamer interface. In the current rendering threshold as in (A), this week interaction cannot be observed; by lowering the threshold, it can be depicted (with the yellow arrow indicating the approximate location of the interaction). In the middle panel, one asymmetric unit is colored and its boundary is highlighted by the dotted red contour.

is based on the proposition made by the previous crystal structures of a single FU, solved in both the oxygen-bound and oxygen-free states, respectively (Cuff et al., 1998; Perbandt et al., 2003). They proposed that the cooperativity effect is attributable to the interactions of two FUs: through one loop directly connected to the active center of one FU and the β strands connected to the active center of another FU.

Biophysical and biochemical evidences have demonstrated that, although the large MH molecular assembly contains very large numbers (160) of oxygen-binding sites, they exhibit relative low cooperativity as measured by the Hill coefficient of around 2 (Decker et al., 2007). Furthermore, when the entire complex disassembles into dimers or single subunit, the oxygen-binding cooperativity disappeared, indicating that even the multiple contacts between the two subunits in the dimer or that in the interface between neighboring FUs in a subunit are not sufficient to impose cooperative oxygen binding (van Holde et al., 2000). Our structure suggests that the "communication clusters" directly responsible for the allosteric effects only exist between FUs of neighboring asymmetric units but not within a single asymmetric unit. These could result in the low cooperativity (Hill coefficient is around 2) relative to other oxygen-binding proteins, which have more extensive subunit-subunit interactions and "allosteric units" (Decker et al., 2007; Cong et al., 2009). Interestingly, this low cooperativity may be responsible for the sluggish movement of the animal in its natural hypoxic environment.

EXPERIMENTAL PROCEDURES

Purification of *Haliotis diversicolor* Hemocyanin

Haliotis diversicolor were cultivated in a South China Sea farm. The hemolymph, harvested according to the methods of Keller (Keller et al., 1999), was centrifuged at 10,000 × *g* for 10 min at 4°C to remove the cells and then ultracentrifuged immediately at 200,000 × *g* for 2 hr at 4°C to sediment the hemocyanins. The supernatant was discarded and the blue hemocyanin pellet was suspended in "stabilizing buffer" (0.2 M NaCl, 50 mM Tris-HCl, 5 mM $CaCl_2$, 5 mM $MgCl_2$ [pH 7.5]).

Purification of HdH Isoform 1

The total HdH was a mixture of HdH1/HdH2 isoforms and had to be further purified to produce a homogeneous sample, which is crucial for high-resolution reconstruction. Anion exchange chromatography using Q-Sepharose and NaCl gradient elution, a method (Harris et al., 2000) for separation of HtH1 from HtH2, was applied here. The major portion of the total HdH, purified HdH1 isoform, was used for our cryo-EM study.

Cryo-EM of HdH1

The HdH1 sample solution (~3 μl) was applied to 1.2/1.3 copper Quantifoil grids (Quantifoil Micro Tools GmbH, Jena, Germany) with a thin continuous carbon film across the holes, blotted by filter papers, and then flash-frozen in precooled ethane using a Vitrobot (FEI, Hillsboro, OR). The sample was imaged on a JEM3200FSC electron cryomicroscope (JEOL, Tokyo) operated at 300 kV and at 60,000× microscope nominal magnification with 20-eV slit of the in-column energy filter. The data were recorded on Kodak SO-163 films with a dose of 20 e/Å^2 per micrograph. The micrographs were digitized using a Nikon Super CoolScan 9000 ED scanner (Nikon, Japan) with 6.35 μm step size with a pixel size of 1.06 Å/pixel on the specimen. The actual pixel size was later recalibrated to be 1.02 Å/pixel by maximizing the cross-correlation between the density map and the starting homology model of the corresponding FUs as previously described (Rossmann, et al., 2001).

Image Processing and 3D Reconstruction

Particle images were automatically boxed out by EMAN2 program *e2boxer.py* (Tang et al., 2007) with a box size of 600 pixels × 600 pixels. Contrast transfer function (CTF) correction was carried out with EMAN1 program *ctfit* (Ludtke et al., 1999). D5 symmetry was confirmed after reference-free 2D image analysis using EMAN1 program *refine2d.py* (Chen et al., 2006) and was imposed in the 3D map reconstruction. All the 3D reconstructions were done with EMAN1, with reference projections in a final angular step of 1.125 degree increment and a soft mask with a Gaussian decay with a five pixel width at the edge of the 3D density. Of the 65,000 original particle images, 28,641 remained in the final reconstruction. Some top and near-top view particles were excluded from the reconstruction due to a preferred orientation of the specimen leading to an excess of these views. In the last five rounds of refinement, the map from the previous round of reconstruction was sharpened using the *proc3d* command with the "*setsf*" option in EMAN1 (Ludtke et al., 1999). This sharpened map was used as the seed map for the last five iterations of projection-matching refinement. A total of about 1,000,000 CPU hours were used for the iterative map refinement. The final resolution was estimated to be 4.5 Å using the 0.5 FSC criterion and the EMAN1 resolution test.

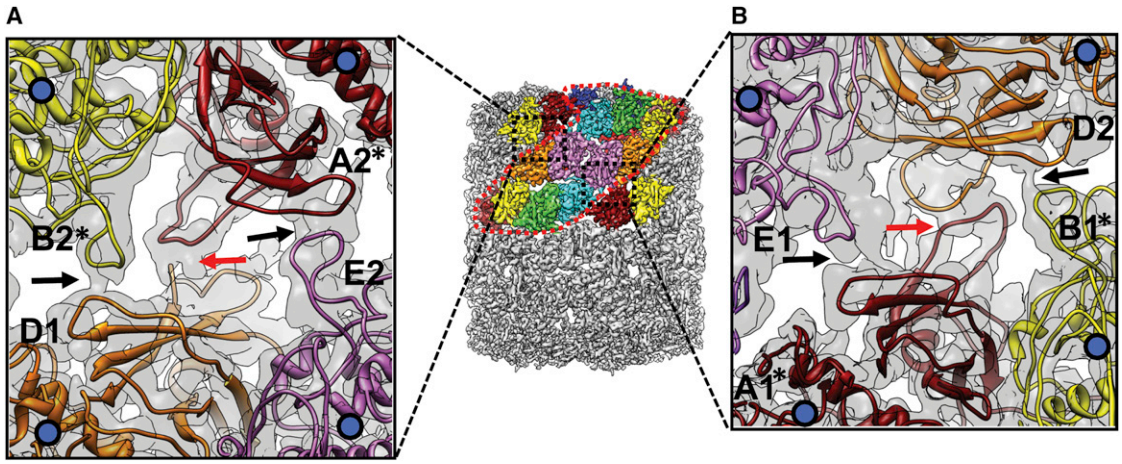

Figure 6. Interactions among Neighboring Asymmetric Units that May Facilitate Communication between the Active Sites

(A) FUs-D1 and E2 in one asymmetric unit (colored and highlighted by the dotted red contour in the middle panel) interact with FUs-B2* and A2* in the neighboring asymmetric unit. There are three linkages (indicated by arrows) in this interface. Among the three linkages, two are formed by loops which directly coupled to the His residues in the oxygen-binding site (black arrow). The third linkage takes place among two β sandwich domains (red arrows), each of which is connected to the oxygen-binding center via Leu as seen in the RtH2e crystal structure.

(B) The same interaction among FUs-D2, E1 of one asymmetric unit (colored and highlighted by the dotted red contour in the middle panel), and the FUs-A1*, B1* of the adjacent asymmetric unit. Interactions shown in (A) and (B) are related by a pseudo 2-fold symmetry of the two subunits (at least for FUs A–F) in the asymmetric unit.

See also Figure S5.

Resolution was further substantiated by comparing the nearly identical subunits within the structure. Segmentations of the individual 16 FUs within an asymmetric unit were done using *Chimera* (Pettersen et al., 2004). The segmentation was straightforward and without ambiguity at this resolution guided by the comparative model. All visualizations were done with *Chimera*. For rigid-body docking, we used the *Chimera* "*fit into map*" module. The FSC between different FUs was calculated in the following way: (1) all the 16 segmented FUs were aligned in *Chimera*; (2) the core regions of each FU were masked out to exclude the apparent disconnected noises around the structure and the connecting loops at the N/C termini of each FU; (3) the FSC curves between these core regions of different FU pairs were then calculated.

Model Building and Segmentation

Sequences of individual FUs including HdH1A to HdH1H (GenBank accession GQ352369) were aligned to that of the homologous OdHg (Cuff et al., 1998) using Clustal W (Thompson et al., 1994). The coordinates of Odg (Cuff et al., 1998) were used as templates to build comparative models for each of HdH1 FUs utilizing Modeller 9v5 (Sali and Blundell, 1993). The models of HdH1 FU-A to FU-H were fitted into the density map using the "*fit into map*" module in *Chimera* (Pettersen et al., 2004). The detailed procedures are as follows. (1) We used a comparative model for each FU to guide the initial segmentation of the map. (2) This model was manually translated and rotated to fit into the density of each FU by matching the secondary structure elements in both the model and the map. This was straightforward due to the clarity of the secondary structure elements in our map. (3) The fitting of the model of the FU was then optimized by using the "*Fit in map*" module in *Chimera*, which maximizes the real space cross correlation between the fitted model and the map. (4) The map of a FU was then segmented out using the "*Zone*" module in *Chimera* with a masking radius of 10 Å, large enough to include all the density belonging to an FU. This process was repeated for each of the 16 FUs within an asymmetric unit.

Overall the match between the model and the density map is quite good except for some loop regions. Further refinement of those loop regions was carried out by utilizing the *loopmodel* class in Modeller, and local refinement was then done using the *regularize zone* module in the Coot software package (Emsley and Cowtan, 2004). Final flexible fitting and refinement of the model was carried out by utilizing the *relax* protocol in Rosetta (DiMaio et al., 2009) to optimize the agreement of the model with the cryo-EM density map of each FU, while maintaining correct stereochemistry. After these steps, we connected all the FUs' models in each subunit, did some minor local refinements around the linker in Coot. A complete Cα model of the entire HdH1 complex was obtained by applying D5 symmetry to the dimer composed of 2 × 8 FUs.

Finally, we used each refined model instead of the initial comparative model to guide the segmentation of its corresponding density again, with a masking radius of 5 Å. These segmented densities were then used to determine the FSC of the 3D densities for each of the corresponding FUs between the two subunits within one asymmetric unit to evaluate the map quality.

ACCESSION NUMBERS

Cryo-EM density maps have been deposited in the Electron Microscopy Data Bank with accession numbers EMD-5585 and EMD-5586 for the HdH1 didecamer and the two subunits in an asymmetric unit; the Cα model for the asymmetric unit of the HdH1 was deposited in the Protein Data Bank with accession number 3J32. The GenBank accession number for the sequence of HdH reported in this paper is GQ352369.

SUPPLEMENTAL INFORMATION

Supplemental Information includes five figures, one table, and two movies and can be found with this article online at http://dx.doi.org/10.1016/j.str.2013.02.018.

ACKNOWLEDGMENTS

This research has been supported by the Science Foundation of the State Key Laboratory of Biocontrol (SKLBC10B05), the National Natural Science Foundation of China (30870480, 31172428, and 41206118), the Earmarked Fund for Modern Agro-industry Technology Research System (CARS-48), Guangdong Province Agricultural Project (2010B20201014), China, and an NIH grant (P41GM103832). We thank the Texas Advanced Computing Center at the University of Texas at Austin for access to the computing resources supported by NSF grant (MCB100112).

Received: September 4, 2012
Revised: February 1, 2013
Accepted: February 3, 2013
Published: March 28, 2013

REFERENCES

Altenhein, B., Markl, J., and Lieb, B. (2002). Gene structure and hemocyanin isoform HtH2 from the mollusc *Haliotis tuberculata* indicate early and late intron hot spots. Gene *301*, 53–60.

Burmester, T. (2001). Molecular evolution of the arthropod hemocyanin superfamily. Mol. Biol. Evol. *18*, 184–195.

Chen, D.H., Song, J.L., Chuang, D.T., Chiu, W., and Ludtke, S.J. (2006). An expanded conformation of single-ring GroEL-GroES complex encapsulates an 86 kDa substrate. Structure *14*, 1711–1722.

Cong, Y., Zhang, Q., Woolford, D., Schweikardt, T., Khant, H., Dougherty, M., Ludtke, S.J., Chiu, W., and Decker, H. (2009). Structural mechanism of SDS-induced enzyme activity of scorpion hemocyanin revealed by electron cryomicroscopy. Structure *17*, 749–758.

Cuff, M.E., Miller, K.I., van Holde, K.E., and Hendrickson, W.A. (1998). Crystal structure of a functional unit from Octopus hemocyanin. J. Mol. Biol. *278*, 855–870.

Decker, H., Hellmann, N., Jaenicke, E., Lieb, B., Meissner, U., and Markl, J. (2007). Minireview: Recent progress in hemocyanin research. Integr. Comp. Biol. *47*, 631–644.

DiMaio, F., Tyka, M.D., Baker, M.L., Chiu, W., and Baker, D. (2009). Refinement of protein structures into low-resolution density maps using rosetta. J. Mol. Biol. *392*, 181–190.

Emsley, P., and Cowtan, K. (2004). Coot: model-building tools for molecular graphics. Acta Crystallogr. D Biol. Crystallogr. *60*, 2126–2132.

Gatsogiannis, C., and Markl, J. (2009). Keyhole limpet hemocyanin: 9-A CryoEM structure and molecular model of the KLH1 didecamer reveal the interfaces and intricate topology of the 160 functional units. J. Mol. Biol. *385*, 963–983.

Gatsogiannis, C., Moeller, A., Depoix, F., Meissner, U., and Markl, J. (2007). *Nautilus pompilius* hemocyanin: 9 A cryo-EM structure and molecular model reveal the subunit pathway and the interfaces between the 70 functional units. J. Mol. Biol. *374*, 465–486.

Gebauer, W., Harris, J.R., Geisthardt, G., and Markl, J. (1999). Keyhole limpet hemocyanin type 2 (KLH2): detection and immunolocalization of a labile functional unit h. J. Struct. Biol. *128*, 280–286.

Gebauer, W., Robin Harris, J., and Markl, J. (2002). Topology of the 10 subunits within the decamer of KLH, the hemocyanin of the marine gastropod Megathura crenulata. J. Struct. Biol. *139*, 153–159.

Harauz, G., and Van Heel, M. (1986). Exact filters for general geometry three dimensional reconstruction. Optik (Stuttg.) *73*, 146–156.

Harris, J.R., Gebauer, W., and Markl, J. (1993). Immunoelectron Microscopy of Hemocyanin from the Keyhole Limpet (*Megathura crenulata*): A Parallel Subunit Model. J. Struct. Biol. *111*, 96–104.

Harris, J.R., Gebauer, W., Söhngen, S.M., Nermut, M.V., and Markl, J. (1997). Keyhole limpet hemocyanin (KLH), II: Characteristic reassociation properties of purified KLH1 and KLH2. Micron *28*, 43–56.

Harris, J.R., Scheffler, D., Gebauer, W., Lehnert, R., and Markl, J. (2000). *Haliotis tuberculata* hemocyanin (HtH): analysis of oligomeric stability of HtH1 and HtH2, and comparison with keyhole limpet hemocyanin KLH1 and KLH2. Micron *31*, 613–622.

Harris, J.R., Meissner, U., Gebauer, W., and Markl, J. (2004). 3D reconstruction of the hemocyanin subunit dimer from the chiton *Acanthochiton fascicularis*. Micron *35*, 23–26.

Helling, F., Shang, A., Calves, M., Zhang, S., Ren, S., Yu, R.K., Oettgen, H.F., and Livingston, P.O. (1994). GD3 vaccines for melanoma: superior immunogenicity of keyhole limpet hemocyanin conjugate vaccines. Cancer Res. *54*, 197–203.

Keller, H., Lieb, B., Altenhein, B., Gebauer, D., Richter, S., Stricker, S., and Markl, J. (1999). Abalone (*Haliotis tuberculata*) hemocyanin type 1 (HtH1). Organization of the approximately 400 kDa subunit, and amino acid sequence of its functional units f, g and h. Eur. J. Biochem. *264*, 27–38.

Kröger, B., Vinther, J., and Fuchs, D. (2011). Cephalopod origin and evolution: A congruent picture emerging from fossils, development and molecules: Extant cephalopods are younger than previously realised and were under major selection to become agile, shell-less predators. Bioessays *33*, 602–613.

Lamy, J., You, V., Taveau, J.C., Boisset, N., and Lamy, J.N. (1998). Intramolecular localization of the functional units of Sepia officinalis hemocyanin by immunoelectron microscopy. J. Mol. Biol. *284*, 1051–1074.

Lieb, B., Altenhein, B., Markl, J., Vincent, A., van Olden, E., van Holde, K.E., and Miller, K.I. (2001). Structures of two molluscan hemocyanin genes: significance for gene evolution. Proc. Natl. Acad. Sci. USA *98*, 4546–4551.

Lieb, B., Gebauer, W., Gatsogiannis, C., Depoix, F., Hellmann, N., Harasewych, M.G., Strong, E.E., and Markl, J. (2010). Molluscan mega-hemocyanin: an ancient oxygen carrier tuned by a ~550 kDa polypeptide. Front. Zool. *7*, 14.

Longenecker, B.M., Reddish, M., Koganty, R., and MacLean, G.D. (1993). Immune responses of mice and human breast cancer patients following immunization with synthetic sialyl-Tn conjugated to KLH plus detox adjuvant. Ann. N Y Acad. Sci. *690*, 276–291.

Ludtke, S.J., Baldwin, P.R., and Chiu, W. (1999). EMAN: semiautomated software for high-resolution single-particle reconstructions. J. Struct. Biol. *128*, 82–97.

Ludtke, S.J., Baker, M.L., Chen, D.H., Song, J.L., Chuang, D.T., and Chiu, W. (2008). De novo backbone trace of GroEL from single particle electron cryomicroscopy. Structure *16*, 441–448.

Meissner, U., Gatsogiannis, C., Moeller, A., Depoix, F., Harris, J.R., and Markl, J. (2007). Comparative 11A structure of two molluscan hemocyanins from 3D cryo-electron microscopy. Micron *38*, 754–765.

Perbandt, M., Guthöhrlein, E.W., Rypniewski, W., Idakieva, K., Stoeva, S., Voelter, W., Genov, N., and Betzel, C. (2003). The structure of a functional unit from the wall of a gastropod hemocyanin offers a possible mechanism for cooperativity. Biochemistry *42*, 6341–6346.

Pettersen, E.F., Goddard, T.D., Huang, C.C., Couch, G.S., Greenblatt, D.M., Meng, E.C., and Ferrin, T.E. (2004). UCSF Chimera—a visualization system for exploratory research and analysis. J. Comput. Chem. *25*, 1605–1612.

Rosenthal, P.B., and Henderson, R. (2003). Optimal determination of particle orientation, absolute hand, and contrast loss in single-particle electron cryomicroscopy. J. Mol. Biol. *333*, 721–745.

Rossmann, M.G., Bernal, R., and Pletnev, S.V. (2001). Combining electron microscopic with x-ray crystallographic structures. J. Struct. Biol. *136*, 190–200.

Sabbatini, P.J., Ragupathi, G., Hood, C., Aghajanian, C.A., Juretzka, M., Iasonos, A., Hensley, M.L., Spassova, M.K., Ouerfelli, O., Spriggs, D.R., et al. (2007). Pilot study of a heptavalent vaccine-keyhole limpet hemocyanin conjugate plus QS21 in patients with epithelial ovarian, fallopian tube, or peritoneal cancer. Clin. Cancer Res. *13*, 4170–4177.

Sali, A., and Blundell, T.L. (1993). Comparative protein modelling by satisfaction of spatial restraints. J. Mol. Biol. *234*, 779–815.

Saxton, W.O., and Baumeister, W. (1982). The correlation averaging of a regularly arranged bacterial cell envelope protein. J. Microsc. *127*, 127–138.

Scheres, S.H., and Chen, S. (2012). Prevention of overfitting in cryo-EM structure determination. Nat. Methods *9*, 853–854.

Siezen, R.J., and van Bruggen, E.F. (1974). Structure and properties of hemocyanins. XII. Electron microscopy of dissociation products of Helix pomatia alpha-hemocyanin: quaternary structure. J. Mol. Biol. *90*, 77–89.

Siezen, R.J., and van Driel, R. (1974). Structure and properties of hemocyanins. XIII. Dissociation of Helix pomatia alpha-hemocyanin at alkaline pH. J. Mol. Biol. *90*, 91–102.

Slovin, S.F., Ragupathi, G., Musselli, C., Fernandez, C., Diani, M., Verbel, D., Danishefsky, S., Livingston, P., and Scher, H.I. (2005). Thomsen-Friedenreich (TF) antigen as a target for prostate cancer vaccine: clinical trial

results with TF cluster (c)-KLH plus QS21 conjugate vaccine in patients with biochemically relapsed prostate cancer. Cancer Immunol. Immunother. *54*, 694–702.

Summers, N.L., Carlson, W.D., and Karplus, M. (1987). Analysis of side-chain orientations in homologous proteins. J. Mol. Biol. *196*, 175–198.

Tang, G., Peng, L., Baldwin, P.R., Mann, D.S., Jiang, W., Rees, I., and Ludtke, S.J. (2007). EMAN2: an extensible image processing suite for electron microscopy. J. Struct. Biol. *157*, 38–46.

Thompson, J.D., Higgins, D.G., and Gibson, T.J. (1994). CLUSTAL W: improving the sensitivity of progressive multiple sequence alignment through sequence weighting, position-specific gap penalties and weight matrix choice. Nucleic Acids Res. *22*, 4673–4680.

van Holde, K.E., Miller, K.I., and van Olden, E. (2000). Allostery in very large molecular assemblies. Biophys. Chem. *86*, 165–172.

van Holde, K.E., Miller, K.I., and Decker, H. (2001). Hemocyanins and invertebrate evolution. J. Biol. Chem. *276*, 15563–15566.

Zhang, X., Settembre, E., Xu, C., Dormitzer, P.R., Bellamy, R., Harrison, S.C., and Grigorieff, N. (2008). Near-atomic resolution using electron cryomicroscopy and single-particle reconstruction. Proc. Natl. Acad. Sci. USA *105*, 1867–1872.

